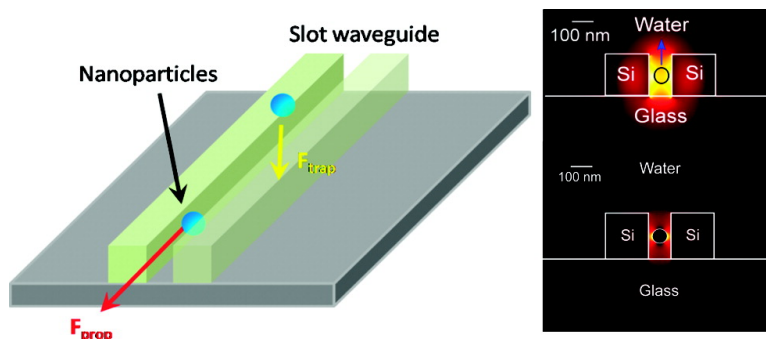


## Forces and Transport Velocities for a Particle in a Slot Waveguide

Allen H. J. Yang, Tadsanapan Lerdsuchatawanich, and David Erickson

*Nano Lett.*, 2009, 9 (3), 1182-1188 • DOI: 10.1021/nl803832q • Publication Date (Web): 29 January 2009

Downloaded from <http://pubs.acs.org> on March 11, 2009



### More About This Article

Additional resources and features associated with this article are available within the HTML version:

- Supporting Information
- Access to high resolution figures
- Links to articles and content related to this article
- Copyright permission to reproduce figures and/or text from this article

[View the Full Text HTML](#)

# Forces and Transport Velocities for a Particle in a Slot Waveguide

Allen H. J. Yang,<sup>†</sup> Tadsanapan Lerdsuchatawanich,<sup>‡</sup> and David Erickson<sup>‡,\*</sup>

*School of Chemical and Biomolecular Engineering, and Sibley School of Mechanical and Aerospace Engineering, Cornell University, Ithaca, New York*

*Received December 18, 2008; Revised Manuscript Received January 14, 2009*

## ABSTRACT

Optofluidic transport seeks to exploit the high-intensity electromagnetic energy in waveguiding structures to manipulate nanoscopic matter using radiation pressure and optical trapping forces. In this paper, we present an analysis of optical trapping and transport of sub-100 nm polystyrene and gold nanoparticles in silicon slot waveguides. This study focuses on the effect of particle size, particle refractive index, and slot waveguide geometry on trapping stability and the resulting transport speed. Our results indicate that stable trapping and transport can be achieved for objects as small as 10 or 20 nm in diameter with as much as a 100 fold enhancement in trapping stiffness over the state of the art.

The field of optofluidics<sup>1,2</sup> focuses on the integration of microfluidic devices with photonic<sup>3</sup> components. Prominent examples of such integration include liquid core ARROW waveguides,<sup>4</sup> hydrodynamically tunable optofluidic lenses,<sup>5</sup> particle manipulations using opto-electronic tweezers,<sup>6</sup> and photothermally driven microfluidic transport.<sup>7</sup> Recently there has been an increased focus in optofluidics as it relates to optical manipulation of micro and nanoparticles in fluidic environments.<sup>8–10</sup> For example, the optical tweezer<sup>11</sup> has been used to manipulate and trap microscale objects,<sup>12</sup> liquid droplets,<sup>13</sup> and even some submicron objects such as viruses<sup>14</sup> and silver nanoparticles.<sup>15</sup> The advantages of optical manipulation include the precision and parallel nature with which matter can be handled and the relatively simple integration of free space optics with chip-based microfluidic devices. Ultimately however, optical tweezers are fundamentally limited by the natural diffraction of light. First, the diffraction limit places an upper bound on how tightly a laser can be focused and by extension the trapping force that can be generated. Second, due to the well-known relationship between spot size and depth of focus, there is a tradeoff between increased focus versus the available interaction length. As such, long distance optical transport of nanoscopic matter using freespace light is very difficult.

One solution to the diffraction limit challenge is in using optical waveguides to confine light within solid structures.<sup>16</sup> Light confined in such a manner is considered a self-consistent wave and can propagate through a waveguide indefinitely without losses or changing its form. As a result

of this unique feature, objects in the optical field of a waveguide can be propelled via radiation pressure along the length of a waveguide for an indefinite distance (not limited by the depth of focus of a laser beam). Solid-core waveguides have been shown to be able to transport a variety of objects such as cells,<sup>17</sup> gold nanoparticles,<sup>18</sup> and submicron polystyrene beads via evanescent field interactions.<sup>19</sup> Previously, Yang and Erickson<sup>20</sup> proposed a numerical finite-element method for studying the trapping stability of submicron particles trapped on solid core waveguides. More recent experimental work has focused on improving the efficiency of waveguides for trapping and transport, with efforts in creating hollow-core<sup>4</sup> and liquid-core<sup>21</sup> waveguides, which allow access to the entire optical mode.

Recently Yang et al.<sup>22</sup> demonstrated the trapping and transport of polystyrene nanoparticles and DNA molecules using slotted silicon waveguides.<sup>23</sup> The slot waveguide, shown in Figure 1a, is comprised of a nanoscale region of low refractive index flanked by two materials of drastically higher refractive index. The high index contrast in the slot region creates a pseudo transverse-electric mode that exhibits large electric field discontinuities at the slot-waveguide boundaries. The effect of the small slot size and the large field discontinuities at the high/low index boundaries generates a high-intensity eigenmode in the slot, such that the majority of the optical energy is confined within the accessible low-index region. The advantage of such a technique is in confining light in the slot cavity of the waveguide, allowing combined hollow-core and liquid-core behavior and creating strong optical intensities and gradients.

In this paper, we examine theoretically the optical trapping and transport of nanoparticles of different composition,

\* To whom correspondence should be addressed. E-mail: de54@cornell.edu.

<sup>†</sup> School of Chemical and Biomolecular Engineering.

<sup>‡</sup> Sibley School of Mechanical and Aerospace Engineering.

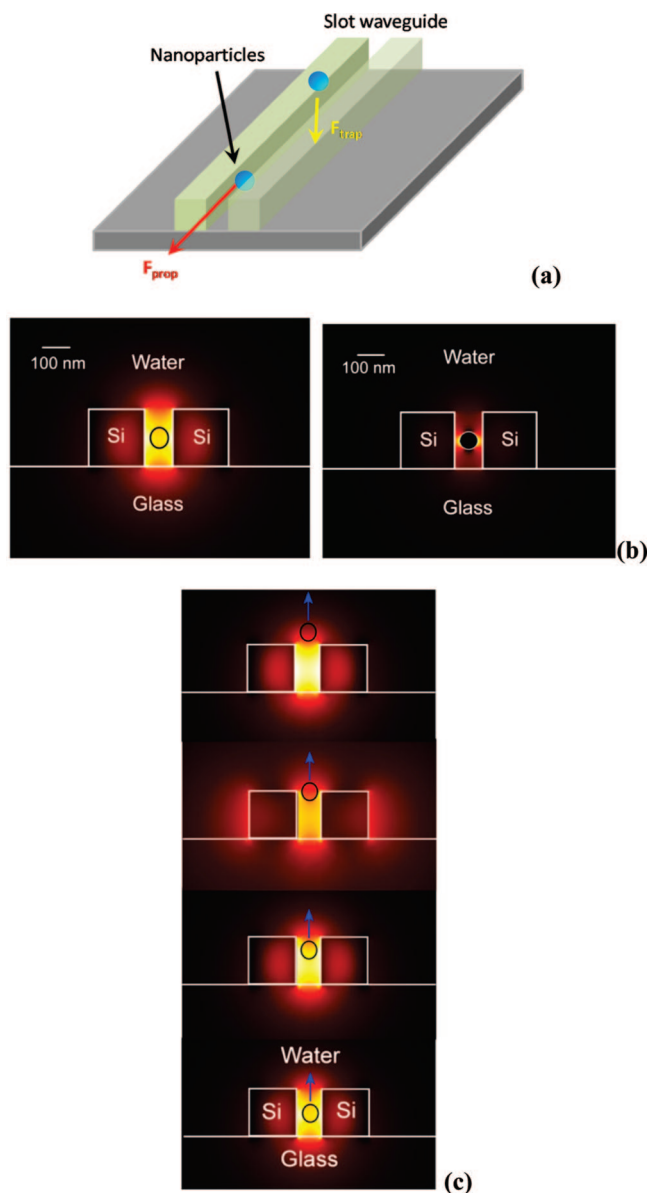


**Figure 1.** Nanophotonic Optofluidic Transport. (a) Schematic of forces acting on nanoparticles in a slot waveguide. (b) Simulation images comparing optical intensity of 65 nm polystyrene and gold nanoparticles in a 100 nm slot waveguide. (c) Compilation of images showing a 65 nm polystyrene nanoparticle as it moves up and out of a slot waveguide.

namely polystyrene and gold in these silicon slotted waveguides. This study is comprised of numerical simulation and analysis of trapping stability and transport velocities for a range of applicable experimental parameters. Our goal here is to discern the practical limits of this method of nanoscale transport. This study focuses on the effect of particle size, particle refractive index, and slot waveguide geometry on trapping stability and the resulting transport speed.

Figure 1a illustrates the slotted waveguide model system used in this study. The waveguide structure itself is fabricated from silicon on a glass substrate. Analogous to the experimental system presented in Yang et al.,<sup>22</sup> a microfluidic channel runs over the slot waveguide transporting particles to the trap. The upper cladding therefore has the properties of water and the lower cladding the properties of silicon

dioxide. The slot region of the waveguide is exposed to the region directly above it, which allows suspended nanoparticles to directly access light propagating through the waveguide. Light at 1550 nm was used here because of the relative transparency of all the materials in the system at that wavelength. We choose to analyze polystyrene particles here because they have a low absorption cross-section and low index contrast relative to water-based environments. In addition, these particles coarsely mimic the properties of organic and biological materials. We also examine the use of gold nanoparticles because of their high absorption cross section and refractive index contrast properties.

In our previous work,<sup>20</sup> we demonstrated that the primary driving force behind trapping stability is that there is a finite work energy required to remove a particle from a stably trapped location to one where the trap no longer has any influence. To summarize

$$S = \frac{W_{\text{trap}}}{k_B T} \quad (1)$$

where  $S$  is the stability number,  $W_{\text{trap}}$  is the work energy required to remove a particle from a trap,  $k_B$  is the Boltzmann constant, and  $T$  is the system temperature. The Boltzmann term,  $k_B T$  is used to represent the random thermal energy of the particle due to Brownian motion. As particle size decreases from micrometer to nanometer dimensions,  $k_B T$  comprises a relatively larger portion of total energy imparted to the particle, resulting in stronger thermal motion. The stability number,  $S$ , can be used to describe the relative strength of an optical trap against such random motion and other external forces, where higher numbers represent stronger traps. For a trap that has a single direction of release, the work can be described as the integral of the forces exerted on the particle as it moves in the direction of release. The electromagnetic force acting on the particle can be described using

$$W_{\text{trap}} = \int \mathbf{F}_{\text{trap}} dx \quad (2)$$

$$\mathbf{F}_{\text{trap}} = \oint_S \langle \mathbf{T}_M \rangle \cdot \mathbf{n} dS \quad (3)$$

where  $\mathbf{F}_{\text{trap}}$  is the trapping force,  $\langle \mathbf{T}_M \rangle$  is the time averaged Maxwell Stress Tensor (MST), and  $\mathbf{n}$  is the normal vector. Interested readers are directed to Yang and Erickson<sup>20</sup> for more information on electromagnetic forces. Furthermore, eq 1 can be used to relate the energy of the trap to a kinetic release rate. We can characterize the rate constant for such a release mechanism using an Arrhenius law

$$k = A \exp\left(-\frac{W_{\text{trap}}}{k_B T}\right) = A \exp(-S) \quad (4)$$

where  $k$  is the particle release rate constant,  $A$  is the Arrhenius constant,  $k_B$  is the Boltzmann constant, and  $T$  is the temperature of the system. Equation 4 can be used as part of a rate law in order to define a relationship between the rate of release of nanoparticles from a slot waveguide trap and the overall strength of the trapping potential. Interested readers are directed to McCann et al.<sup>24</sup> or Kolasinski<sup>25</sup> for more detailed information regarding nanoparticle escape from trapping potentials.

**Table 1.** Simulation and Geometric Parameters

domain	material	domain size <sup>a</sup>	refractive index
waveguide	silicon	200 × 200 nm (each)	3.48
slot width	water	100 nm/40 nm	1.33
substrate	silicon dioxide	lower subdomain	1.45
microfluidic channel	water	indefinite	1.33
particle A	polystyrene	10 – 65 nm	1.55
particle B	gold	10 – 65 nm	0.18 + 10.21i

<sup>a</sup> Waveguide dimensions given as cross-section.

We can also find the steady state velocity for a particle in a slot waveguide by equating the propulsion forces ( $\mathbf{F}_{\text{Prop}}$ ) with the hydrodynamic drag force ( $\mathbf{F}_{\text{Drag}}$ ).

$$\mathbf{F}_{\text{Prop}} = \mathbf{F}_{\text{Drag}} \quad (5)$$

$$\mathbf{F}_{\text{Drag}} = C_{\text{Drag}} \mathbf{U} \quad (6)$$

$$\mathbf{U} = \frac{\mathbf{F}_{\text{Prop}}}{C_{\text{Drag}}} \quad (7)$$

where  $\mathbf{F}_{\text{Prop}}$  is the force of scattered and absorbed photons on a particle,  $\mathbf{F}_{\text{Drag}}$  is the hydrodynamic drag on a particle,  $C_{\text{Drag}}$  is the drag coefficient of the particle, and  $\mathbf{U}$  is the steady state velocity. For the case of a sphere moving through a stagnant fluid,  $C_{\text{Drag}}$  is the Stokes drag coefficient  $6\pi\eta a$ , where  $\eta$  is the fluid viscosity and  $a$  is the particle radius. For a particle close to a surface, a near wall correction can be added to account for close proximity to a flat surface.<sup>26</sup> The most accurate method, which is used in our analysis, is through simulation of the particle/geometry domain and determining  $C_{\text{Drag}}$  numerically. To determine this here all parallel boundaries surrounding the nanoparticle are assigned a negative slip velocity to simulate the movement of a nanoparticle through the slot waveguide. Given the slip velocity and  $\mathbf{F}_{\text{Drag}}$  from this simulation  $C_{\text{Drag}}$  can be computed from eq 5.

Numerical calculations were conducted using a finite-element method. Geometric parameters for the simulations used in our case studies are listed in Table 1. Here we outline our methods for calculating the steady-state electric and velocity fields and the determination of the optical forces and hydrodynamic drag on spherical nanoparticles in slotted waveguides, along with our key assumptions. The electromagnetic field distribution in a slotted waveguide is determined by solving Maxwell's equations for the waveguide geometry, including the upper and lower cladding regions. A perfectly matched layer (PML) region is added to the output boundary of the geometry to absorb incoming radiation with minimal reflection. The input field distribution is determined by the solution of a boundary mode eigenvalue solver. The surrounding boundaries allow for a nonzero flux of scattered light, as expected for an unbounded cladding region. We determine the steady-state velocity field through the solution of the Stokes' equations, assuming incompressible flow and a viscous flow, which characterizes low Reynolds number flow in a microchannel. The input and output boundaries enforce a zero normal stress condition.

In our simulations, we assume that the relevant electromagnetic and hydrodynamic equations can be decoupled, and thus the optical and drag forces can be computed independently of each other. We do not consider the effect of absorption of light at 1550 nm by the water surrounding the

waveguide. In an experimental system, however, the maximum power available would be limited by the amount of heat that is absorbed. One method for dealing with high water absorption is in using deuterium oxide (heavy water) for the fluid medium, which has a significantly lower absorption at 1550 nm.<sup>27</sup> We also neglect the effects of electrical double layer (EDL) repulsion. We do state that an aqueous solution at an ionic strength of 100 mM would have a characteristic repulsion range of approximately 1 nm, which is smaller than the length scales involved in our model.

Numerical validation (experimental validation is provided below) of the finite element simulation method was accomplished by creating a simulation that would mimic the conditions of a uniform plane wave incident on a nanoparticle. The simulation domain consists of a cube containing liquid water with a dielectric nanoparticle suspended in the center of the cube. Surrounding the box region are perfectly matched layer PML boundaries designed to absorb all scattered and incident light. Using this geometry, we simulated the effects of a plane wave as it scatters off the nanoparticle and the scattering force on the nanoparticle. Shown in Figure 2, we plot the results of these simulations against calculated results using the Rayleigh scattering equation, changing only the particle diameter in subsequent iterations. As expected, we note that there is an insignificant amount of force generated in directions orthogonal to optical propagation. However, for particles above 100 nm in diameter, deviations appear in simulated values compared to Rayleigh theory. Shown in Figure 2b, plotting the convergence between simulated and calculated values versus the Rayleigh criterion ( $D\pi/\lambda \ll 1$ ), where  $D$  is the particle diameter and  $\lambda$  is the freespace wavelength, we see that as  $D\pi/\lambda$  gets larger, convergence between the two methods decreases. This agrees with similar calculations conducted for particle propulsion on silicon nitride waveguides<sup>28</sup> and our previous work<sup>19,20</sup> that observed size dependences much lower than the predicted sixth order and third order dependencies for Rayleigh scattering and gradient forces.

As stated previously, in this study we seek to determine practical limits for nanophotonic optofluidic transport. Figure 3 illustrates the trapping forces exerted on polystyrene and gold nanoparticles for varying vertical positions in the waveguide structure. Qualitatively, we note three key features of these force profiles. Particles that are positioned below the median of the waveguide structure (100 nm) tend to exhibit a net upward force, while particles positioned above the median point exhibit a net downward force. This suggests that the optical gradient in the waveguide tends to guide particles toward the middle of the structure where the

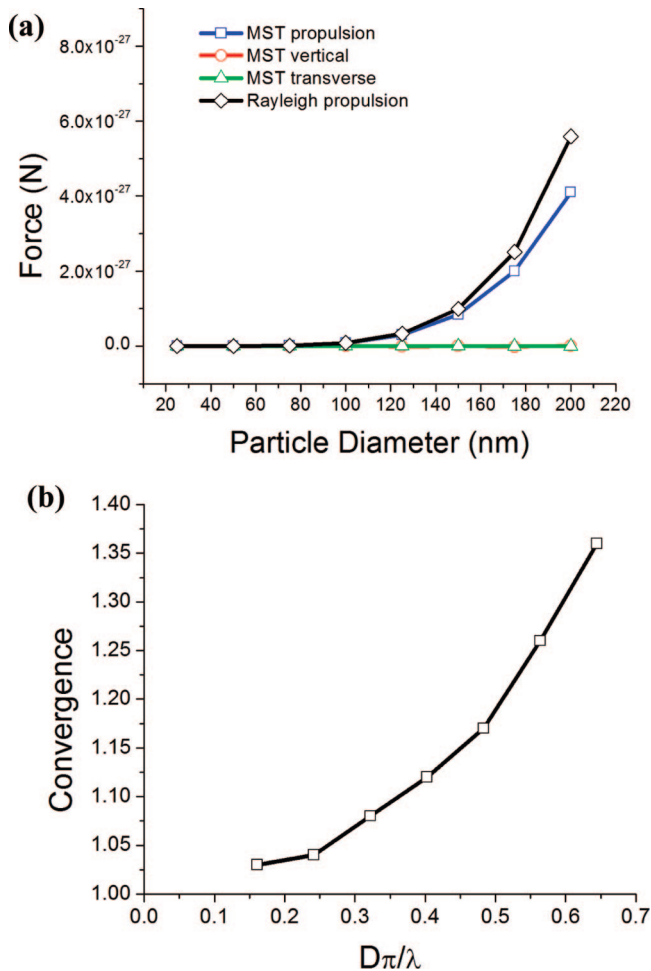


**Figure 2.** Comparison of MST to Rayleigh scattering. (a) Plot of simulated optical force due to a plane wave incident on a particle and calculated forces using the Rayleigh scattering equation for increasing particle sizes. (b) Plot of convergence ( $1 - F_{\text{MST}}/F_{\text{Ray}}$ ) versus the Rayleigh criterion ( $D\pi/\lambda$ ).

intensity is at its maximum. A second feature we observe is that the trapping force attains its maxima in all profiles at a height of 200 nm corresponding to the height of the waveguide. Once the trapping force has reached its maxima, it decays rapidly to zero, which is representative of the fast decline of the evanescent wave behaving regions of the waveguide structure. The characteristic decay length of the force profiles appears to be on the order of 50–100 nm, which is much shorter than previously reported results for particles on single mode waveguides.

Several observations can be made regarding the sensitivity of the trapping force with respect to the variables of interest. As expected, particles of increasing diameter experience stronger trapping forces in the slot waveguide. This sensitivity also is stronger than previously reported results for microspheres and larger submicrometer objects with similar refractive index.<sup>17,20</sup> The increased dependence results from the much smaller nanoparticles used in this study that more closely approximate Rayleigh particles and thus come closer to exhibiting the theoretical third order sensitivity to particle size. The calculated force profiles for gold nanoparticles, shown in Figure 3b, showed stronger trapping compared to

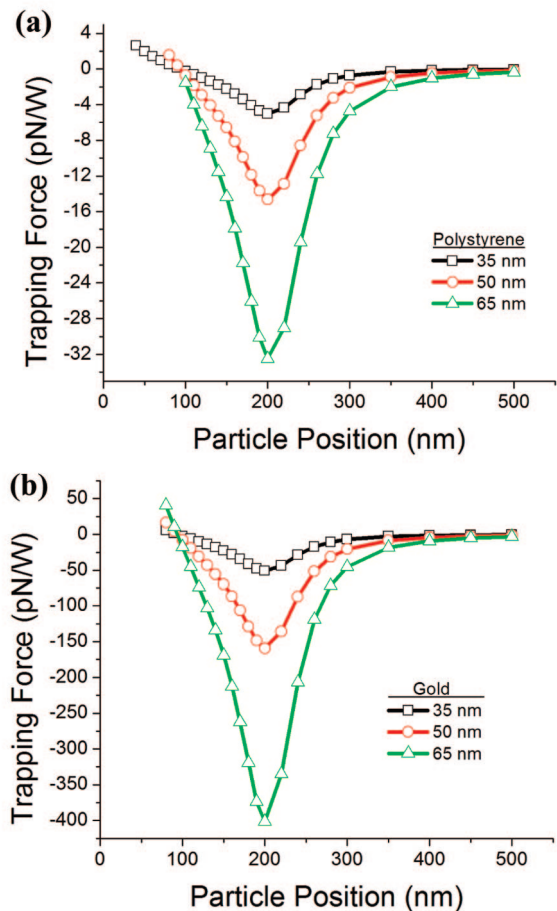


**Figure 3.** Trapping forces on nanoparticles in a 100 nm slot. Plots of trapping forces for particles at varying vertical position within the slot waveguide for (a) polystyrene nanoparticles and (b) gold nanoparticles.

polystyrene beads of the same size. This effect can be attributed to the relatively large refractive index contrast between water and gold.

Figure 4a shows the propulsion force profiles for gold particles in slot waveguides. We see similar dependences on size to those in Figure 3 with some differences. The size sensitivity of the propulsion force profiles is much more pronounced in comparison to the trapping force, power law fits of the average propulsion velocities yield a sixth order relationship with respect to size, which is consistent with Rayleigh theory. Figure 4c, which shows the optical intensity in a slot waveguide, illustrates the strong proportionality between intensity and the propulsion forces exerted upon it, which is predicted by Rayleigh theory. Direct propulsion force values for polystyrene nanoparticles could not be obtained, because the values were several orders of magnitude below the numerical resolution. We can however extend the Rayleigh particle assumption to polystyrene particles (within the regime validated by the results presented in Figure 2) and calculate the scattering forces exerted upon them as shown in Figure 4b. As expected, we find that the propulsion forces exerted on a polystyrene particle is many orders of magnitude smaller than the gold nanoparticles.

There are also significant effects from decreasing slot width, resulting in an increase the optical intensity in the

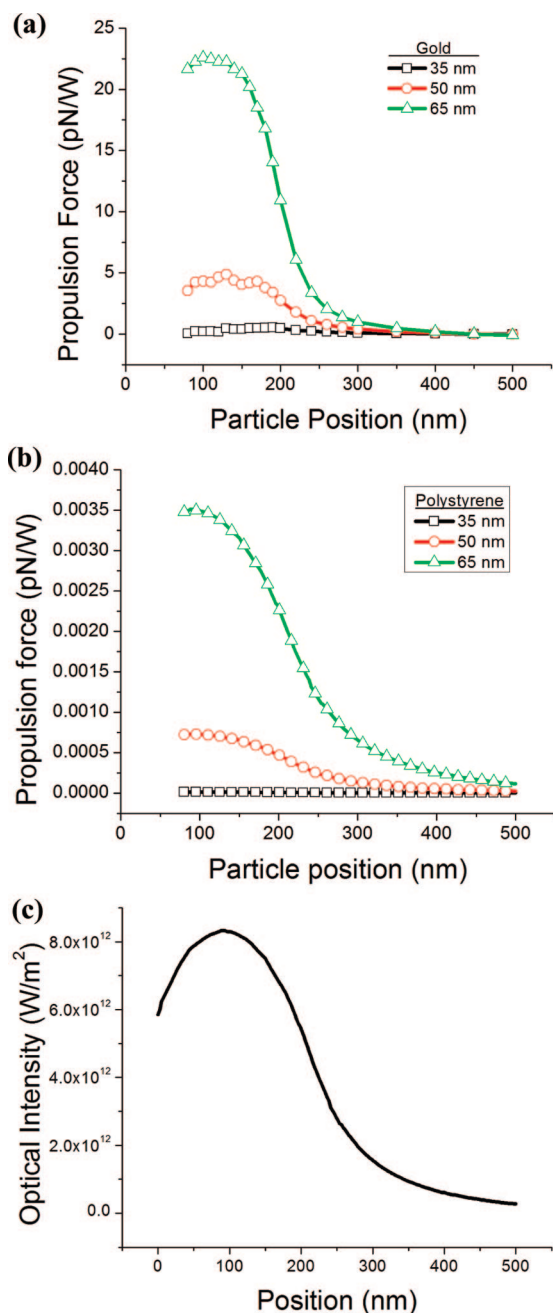


**Figure 4.** Propulsion forces on nanoparticles in a 100 nm slot. Plots of propulsion forces (in the direction of optical propagation) of particles at varying vertical positions within the slot waveguide for (a) gold nanoparticles and (b) polystyrene nanoparticles. The polystyrene propulsion force values were obtained by calculating the scattering force on the particles given the optical intensity profile within the waveguide assuming Rayleigh scattering. (c) Optical intensity in the waveguide as a function of the vertical position.

waveguide, shown in Figure 5. Unlike the trapping profiles for the larger nanoparticles (Figure 3), we notice a very sharp increase in the trapping force as the particle position approaches the lip of the slot waveguide. Simulations show that in the larger 100 nm slot, the calculated trapping forces for 10 and 20 nm particles are relatively small. However, in a 30 nm slot, the trapping forces increases to values approximate to those of larger nanoparticles in the 100 nm slot system. We also notice a very sharp increase in the

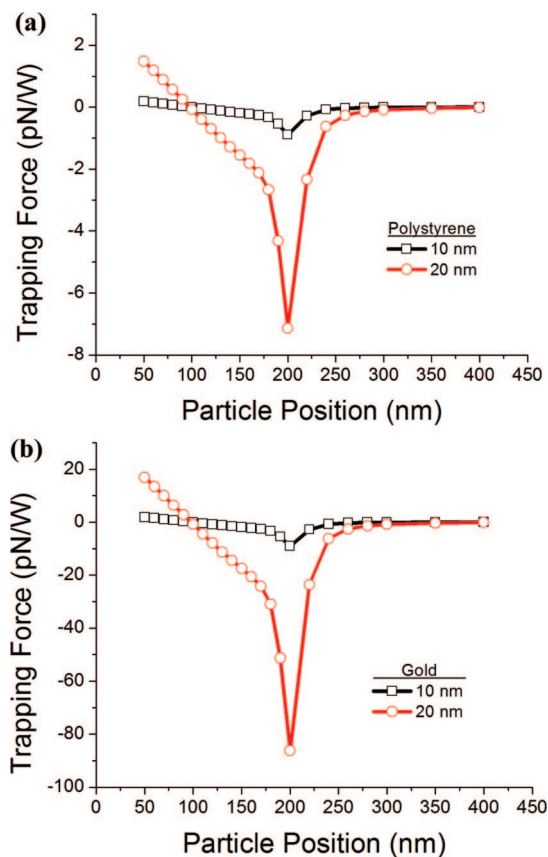


**Figure 5.** Trapping force for nanoparticles in a 30 nm slot. Trapping forces exerted on nanoparticles in a 30 nm slot for (a) polystyrene nanoparticles and (b) gold nanoparticles.

trapping force as the particle position approaches the lip of the slot waveguide. As such, increasing or decreasing the slot width is a controllable parameter that can variably tune the trapping force to more effectively target smaller or larger targets.

From the data provided from Figures 3 and 4, we can calculate the stability numbers and steady state velocities using eqs 1 and 6 described previously. These results are summarized in Table 2. Assuming ideal coupling, the threshold power outlines the required coupled power in a slotted waveguide in order to achieve a stability number equal to 1, which is the minimum value of  $S$  required to trap a particle. Considering losses in experimental systems and that we do not consider any bulk fluid flow in our model, our predictions here underestimate the amount of power required for optical trapping in a slot waveguide. Even with these numbers, we observe trapping a 10 or 20 nm object with a refractive index contrast similar to or smaller than polystyrene would be near impossible due to the relatively large power requirements. However, because of the higher refractive index contrast between gold and water, we believe it is experimentally viable to trap colloidal gold particles in slotted waveguides with very small widths.

We also tabulate the calculated values of the trap stiffness, obtained by calculating the slope of the trapping force profile. On the basis of previously reported values for trapping stiffness in a plasmonic tweezer experiment of 0.013 pN/

**Table 2.** Stability, Trapping Stiffness, and Steady State Velocities

particle material	diameter <sup>a</sup> (nm)	stability number (W <sup>-1</sup> )	threshold power (mW)	trap stiffness (pN/nm/W)	average velocity ( $\mu\text{m/s/W}$ )
polystyrene	65	875	1.14	1.25	29.6
	50	392	2.55	0.556	9.81
	35	122	8.19	0.188	0.275
	20	140	7.14	0.131	
	10	17.3	57.8	0.01624	
gold	65	9890	0.101	14.2	13800
	50	4120	0.243	5.82	4530
	35	1330	0.75	1.89	716
	20	1590	0.628	1.50	
	10	174.2	5.74	0.164	

<sup>a</sup> Table values for 10 and 20 nm diameter particles were calculated using 30 nm slot width.

nm/W (upper limit value)<sup>29</sup> for 200 nm polystyrene particles, we predict our system has an enhancement of about 100 $\times$  for particles of similar composition and size. Also, experimental results for the trapping of gold nanoparticles in optical tweezers reports trapping stiffness values approximately 100 times smaller than our predicted values using a slotted waveguide.<sup>30</sup> Table 2 also lists the calculated steady state velocities for the different sized particles. In this analysis, we use the values for average propulsion force and particle drag in the slot structure. Just as with the threshold power, these values here represent ideal values where coupling losses and losses in the waveguide would result in a loss of efficiency in the system. Within these limitations, we can see that for low refractive index contrast materials, optofluidic propulsion for objects below a diameter of 50 nm is very small due to the size sensitivity of the scattering force. Table 2 also lists the calculated steady state velocities for the smaller set of nanoparticles. In this analysis, we use the values for average propulsion force and particle drag in the slot structure. Just as with the threshold power, these values here represent ideal values where coupling losses and losses in the waveguide would result in a loss of efficiency in the system. With these limitations, optofluidic propulsion for objects with low refractive index contrast below a diameter of 50 nm is very small due to the size sensitivity of the scattering force.

Using data from experiments and the devices previously detailed in Yang et al.,<sup>22</sup> we can compare our predicted values to experimental measurements of steady-state velocities of nanoparticles in slot waveguides in order to validate the above predictions. The average speed of the 100 nm diameter polystyrene spheres was found to be  $2.3 \pm 2.5 \mu\text{m/s}$ . In those experiments, an input power of 250 mW light at 1550 nm was used with a measured output of 1 mW. Assuming a  $-3$  dB coupling loss, and a uniform loss per unit distance over the length of the chip with the slot waveguide position about 3 mm from the edge of a 1 cm long waveguide, we estimate approximately 25 mW was coupled into the slot waveguides. Using the same methods described earlier to calculate the values in Table 2, but with modifications in the simulations to account for a 100 nm polystyrene bead in a 140 nm slot waveguide, we calculate the steady-state velocity to be  $1.3 \mu\text{m/s}$  at 25 mW of guided power, which is of the same order as that predicted by our model. The discrepancy between the two results is most likely due to the inability to get an accurate measure of the actual power at the slot location in

the experiments and the relatively large spread in the observed transport velocities.

In conclusion, we have shown through our analysis and simulation results that the trapping and transport of nanoscale species of both low and high refractive index contrasts are possible. Our model accounts for a number of factors such as increased Brownian motion for particles with dimensions below 100 nm. Our results also highlight potential system changes such as slot width or particle refractive index that can be used to alter the expected trapping stability and transport speeds.

**Acknowledgment.** The authors thank Professor Abraham Stroock for critical discussions. This work was funded by the U.S. National Science Foundation NIRT: Active Nanophotofluidic Systems for Single Molecule/Particle Analysis (Award number 0708599).

**Supporting Information Available:** This material is available free of charge via the Internet at <http://pubs.acs.org>.

## References

- (1) Psaltis, D.; Quake, S. R.; Yang, C. H. *Nature* **2006**, *442* (7101), 381–386.
- (2) Monat, C.; Domachuk, P.; Eggleton, B. J. *Nat. Photonics* **2007**, *1* (2), 106–114.
- (3) Saleh, B. E. A.; Teich, M. C. *Fundamentals of photonics*; Wiley: New York, 1991.
- (4) Measor, P.; Kuehn, S.; Lunt, E. J.; Phillips, B. S.; Hawkins, A. R.; Schmidt, H. *Opt. Lett.* **2008**, *33* (7), 672–674.
- (5) Mao, X. L.; Waldeisen, J. R.; Juluri, B. K.; Huang, T. J. *Lab Chip* **2007**, *7* (10), 1303–1308.
- (6) Chiou, P. Y.; Ohta, A. T.; Wu, M. C. *Nature* **2005**, *436* (7049), 370–372.
- (7) Liu, G. L.; Kim, J.; Lu, Y.; Lee, L. P. *Nat. Mater.* **2006**, *5* (1), 27–32.
- (8) Applegate, R. W.; Squier, J.; Vestad, T.; Oakey, J.; Marr, D. W. M.; Bado, P.; Dugan, M. A.; Said, A. A. *Lab Chip* **2006**, *6* (3), 422–426.
- (9) Grujic, K.; Helleso, O. G.; Hole, J. P.; Wilkinson, J. S. *Opt. Express* **2005**, *13* (1), 1–7.
- (10) Marchington, R. F.; Mazilu, M.; Kuriakose, S.; Garcés-Chávez, V.; Reece, P. J.; Krauss, T. F.; Gu, M.; Dholakia, K. *Opt. Express* **2008**, *16* (6), 3712–3726.
- (11) Ashkin, A. *Phys. Rev. Lett.* **1970**, *24* (4), 156.
- (12) Ashkin, A.; Dziedzic, J. M.; Bjorkholm, J. E.; Chu, S. *Opt. Lett.* **1986**, *11* (5), 288–290.
- (13) Jones, P. H.; Stride, E.; Saffari, N. *Appl. Phys. Lett.* **2006**, *89* (8), 081113.
- (14) Ashkin, A.; Dziedzic, J. M. *Science* **1987**, *235* (4795), 1517–1520.
- (15) Bosanac, L.; Aabo, T.; Bendix, P. M.; Oddershede, L. B. *Nano Lett.* **2008**, *8* (5), 1486–1491.
- (16) Pollock, C. R.; Lipson, M. *Integrated photonics*; Kluwer Academic: Boston, 2003.
- (17) Gaugiran, S.; Getin, S.; Fedeli, J. M.; Colas, G.; Fuchs, A.; Chatelain, F.; Derouard, J. *Opt. Express* **2005**, *13* (18), 6956–6963.

- (18) Ng, L. N.; Luff, B. J.; Zervas, M. N.; Wilkinson, J. S. *Opt. Commun.* **2002**, *208* (1–3), 117–124.
- (19) Schmidt, B. S.; Yang, A. H.; Erickson, D.; Lipson, M. *Opt. Express* **2007**, *15* (22), 14322–14334.
- (20) Yang, A. H. J.; Erickson, D. *Nanotechnology* **2008**, *19* (4), 045704.
- (21) Wolfe, D. B.; Conroy, R. S.; Garstecki, P.; Mayers, B. T.; Fischbach, M. A.; Paul, K. E.; Prentiss, M.; Whitesides, G. M. *Proc. Natl. Acad. Sci. U.S.A.* **2004**, *101* (34), 12434–12438.
- (22) Yang, A. H. J.; Moore, S. D.; Schmidt, B. S.; Klug, M.; Lipson, M.; Erickson, D. *Nature* **2009**, *457* (7225), 71–75.
- (23) Almeida, V. R.; Xu, Q. F.; Barrios, C. A.; Lipson, M. *Opt. Lett.* **2004**, *29* (11), 1209–1211.
- (24) McCann, L. I.; Dykman, M.; Golding, B. *Nature* **1999**, *402* (6763), 785–787.
- (25) Kolasinski, K. *Surface Science: Foundations of Catalysis and Nanoscience*; John Wiley & Sons Ltd: West Sussex, England, 2002.
- (26) Svoboda, K.; Block, S. M. *Annu. Rev. Biophys. Biomol. Struct.* **1994**, *23*, 247–285.
- (27) Armani, A. M.; Vahala, K. J. *Opt. Lett.* **2006**, *31* (12), 1896–1898.
- (28) Gaugiran, S.; Gétin, S.; Fedeli, J. M.; Derouard, J. *Opt. Express* **2007**, *15* (13), 8146–8156.
- (29) Grigorenko, A. N.; Roberts, N. W.; Dickinson, M. R.; Zhang, Y. *Nat. Photonics* **2008**, *2* (6), 365–370.
- (30) Hansen, P. M.; Bhatia, V. K.; Harrit, N.; Oddershede, L. *Nano Lett.* **2005**, *5* (10), 1937–1942.

NL803832Q